Applied Surface Science 485 (2019) 476–483

Contents lists available at ScienceDirect

Applied Surface Science

journal homepage: www.elsevier.com/locate/apsusc

Full length article

Pt-modified dendritic gold as a highly efficient photoelectrocatalyst for the formic acid oxidation reaction

Feng-Hsuan Cho[a], Min-Hui Huang[a], Yu-Mei Chen[a], Yu-Bin Huang[a], Chun-Jen Su[b], U-Ser Jeng[b,c], Ying-Huang Lai[a,*]

[a] Department of Chemistry, Tunghai University, No. 1727, Sec. 4, Taiwan Boulevard, 40704 Taichung, Taiwan
[b] National Synchrotron Radiation Research Center, Hsinchu 30076, Taiwan
[c] Chemical Engineering Department, National Tsing-Hua University, Hsinchu 30013, Taiwan

ARTICLE INFO

Keywords:
Formic acid oxidation
Underpotential deposition
Pt-modified gold dendrites
Dehydrogenation pathway
Photoelectrocatalysis

ABSTRACT

Sub-monolayer Pt-modified Au dendrites (Au-Ds) were successfully synthesized and characterized using several techniques. The resulting Pt-modified Au-Ds effectively combined component catalytic properties and plasmonic optical properties. Results obtained from comprehensive kinetics experiments revealed that Pt-modified Au-Ds serve as an ideal photoelectocatalyst for the formic acid oxidation reaction (FAOR). Electro- and photoelectrocatalytic FAOR was carried out via the same dehydrogenation pathway on a high-efficiency Pt-modified Au-D surface with a low activation energy of 35.4 kJ mol^{-1}. The contribution from the photo-enhanced electrocatalytic effect reached 68% in the Tafel region. Photoelectrocatalysis and the photo-thermal effect synchronously boosted the FAOR on Pt-modified Au-Ds under illumination. Chronoamperometry results indicated that Pt-modified Au-Ds exhibit excellent stability and long-term durability for the FAOR.

1. Introduction

Owing to climate changes and the limited availability of fossil fuels, the development of clean, low-carbon energy is gradually becoming an urgent, important issue. In recent years, the simplest carboxylic acid, i.e., formic acid, has been used as an important fuel with or without reformation. As direct formic acid fuel cells (DFAFCs) exhibit better efficiency compared to proton-exchange membrane fuel cells and reversible hydrogen storage systems, formic acid could serve as a better fuel for portable devices, vehicles, and other energy-related applications in the future. Hence, the investigation of durable catalysts with high activity for DFAFCs has become the most important task.

Pt and Pt based materials have been confirmed to be the most efficient catalysts for the formic acid oxidation reaction (FAOR); however, because of their high cost, poor durability, and susceptibility to carbon monoxide poisoning, their use for the practical commercialization of DFAFCs is considerably hindered. Typically, the electrocatalysis of the FAOR on Pt-based catalysts follows a dual mechanism, namely, dehydrogenation and dehydration pathways, respectively [1,2]. For DFAFCs, dehydrogenation is a desired reaction pathway to boost the overall cell efficiency. On the other hand, the intermediate-adsorbed carbon monoxide is the species that poisons the electrocatalytically active surface of the Pt catalyst via an undesired dehydration pathway [3–6]. Hence, it is crucial to design a Pt-based catalyst with excellent CO tolerance. To improve the performance and durability of the Pt catalyst, binary, ternary, and even tertiary component materials, such as Pt-Ru, Pt-Pd, Au-Pt, and Pt–Ru–W, have been extensively investigated [7–15]. Among these catalysts, the deposition of a relatively small amount of Pt on the Au surface has been reported to improve the electrocatalytic properties of metal electrodes. [15–17] Reducing the Pt amount of Au-Pt catalysts clearly suppresses the dehydration pathway in the FAOR [16–18]. The detailed reaction mechanism still needs to be understood for the development of advanced catalysts for the FAOR in DFAFCs. On the other hand, plasmon-driven catalytic reactions have attracted considerable attention because of the creation of a new route to control catalytic reactions on metallic substrates [19,20]. The surface plasmon resonance (SPR) effect of nanostructured Au can provide a beneficial electric field nearby to facilitate the separation of photo-excited carriers and to enhance photoelectrocatalytic performance. Zheng et al. demonstrated plasmon-induced interfacial interaction in Pd-modified Au nanorods, which is the main factor that drives plasmon-enhanced catalytic activity [21]. Notably, a finite-difference time-domain (FDTD) simulation revealed that the SPR-induced enhancement is mainly located at the tips of the nanostructured Au, which directed

* Corresponding author.
E-mail address: yhlai@go.thu.edu.tw (Y.-H. Lai).

https://doi.org/10.1016/j.apsusc.2019.04.229
Received 2 January 2019; Received in revised form 19 April 2019; Accepted 24 April 2019
Available online 25 April 2019
0169-4332/ © 2019 Elsevier B.V. All rights reserved.

more efficient use of SPR energy [19]. However, the SPR effect of Pt-modified nanostructured Au has been applied in the FAOR only in a few studies [22]. Accordingly, the binary component catalyst, involving the combination of photo-active nanostructured Au and catalytic active Pt, is expected to exhibit significantly good photoelectrocatalytic activities toward the FAOR. Although all the aforementioned studies observes the dehydrogenation pathway in their electrocatalytic experiments, to the best of our knowledge, photoelectrocatalytic FAOR have not yet been performed with Pt-modified Au catalysts.

In this study, the underpotential deposition (UPD) of copper and platinum redox replacement were employed to prepare a Pt submonolayer on the gold dendrite (Au-D) surface [23,24]. Au-D nanostructures exhibit a high surface-area-to-volume ratio and low density, as well as provide considerable access to electrochemical reactants and a synergistic electrocatalytic effect. [14,25] A Pt adlayer was deposited on the Au-D surface to minimize the amount of Pt on the catalyst. Therefore, an extremely high amount of Pt is utilized in these electrocatalysts as the active sites are only located on the catalyst surface. In addition, Au-Ds exhibit special textured nanostructures, such as sharp edges or tips, and high surface areas, which demonstrate potential applications in catalysis [26]. Then, realize the SPR effect of the photoelectrocatalyst in the FAOR. The reaction kinetics and performance of photo-enhanced fuel cells based on Pt-modified Au-Ds catalysts were examined.

2. Experimental

2.1. Synthesis of Pt-modified Au-Ds and Pt-modified Au-film

Au-Ds were synthesized according to a previously reported study [26–29]. The electrodeposition of Au was performed on a glassy carbon electrode (GCE) in an aqueous solution of 1.0 mM $HAuCl_4$ and 0.5 M H_2SO_4 in the presence of 0.1 mM cysteine. A conventional three-electrode system in an electrochemical workstation (CHI 614B) was employed for electrodeposition. A saturated calomel electrode (SCE) served as a reference electrode; the counter electrode was a platinum wire. Square-wave potential pulses were applied to the GCE at a frequency of 5 s^{-1} for 3000 s [27]. A pulsed potential form was used to reduce the effect of diffusion limits on the electrodeposition rate. Lower and higher potentials of the square-wave pulse with respect to the SCE were set at −0.8 and + 0.2 V, respectively [26]. A copper monolayer was electrodeposited on the Au-D surface at 0 mV in the UPD region [23,24,26]. The UPD of Cu on Au-D/GCE was performed in 0.1 M H_2SO_4 containing 1.0 mM $CuSO_4$. Immediately after deposition, the Cu-modified Au-D/GCE was rapidly dipped into deaerated H_2PtCl_6 in a 0.05 M H_2SO_4 solution for 10 min to replace the Cu layer with Pt via redox replacement. In addition, a copper monolayer was electrodeposited on a Au plate surface at 0 mV in the UPD region. Then the UPD-Cu-modified Au-plate was dipped into deaerated H_2PtCl_6 in a 0.05 M H_2SO_4 solution for 10 min to replace the Cu layer with Pt via redox replacement.

2.2. SEM measurements

FE-SEM images were recorded on a JSM-6700F microscope operated at an accelerating voltage of 3.0 kV.

2.3. XRD measurements

Powder XRD images were recorded on the BL23A XRD end station of the National Synchrotron Radiation Research Center (NSRRC), Taiwan, with an X-ray wavelength λ of 0.775 Å (16 keV) [30]. Powder XRD data were recorded on an image plate, and the diffraction angle 2θ was calibrated by using diffractions from powder mixtures of silicon and silver behenate.

2.4. XPS measurements

XPS profiles were recorded at the SPEM end station of the NSRRC beamline 09A1 [26]. The onset of photoemission from a Au foil attached to the sample holder was used to calibrate the Fermi level as the zero-binding energy. The Au and Pt XPS spectra of the Pt-modified Au-Ds were recorded by using an incident beam of X-ray energy at 580 eV.

2.5. Electrochemical measurements

2.5.1. Cyclic voltammetry

The surface areas of Au-Ds Pt-modified Au plate and Pt-modified Au-Ds/GCE were estimated from cyclic voltammetry (CV) scans by soaking the Au-D/GCE in a N_2-saturated H_2SO_4 solution (0.50 M) at a scan rate of 50 mV/s. CV curves were recorded between −0.40 and 1.5 V versus SCE at ambient temperature. The electrochemically active surface areas (ECSAs) of Pt on Pt-modified Au-Ds/GCE were estimated by hydrogen adsorption/desorption and columbic integration of the enhanced cathodic peak current.

2.5.2. Formic acid oxidation reaction

To examine the electrode catalytic activity, the oxidation of formic acid on the Pt-modified Au-Ds was examined in an aqueous solution (saturated with N_2) of 0.5 M H_2SO_4 and 0.05–0.50 M formic acid. The reactor was immersed into a temperature controlled water bath. CV curves were recorded between −0.2 and 1.0 V versus SCE at a scan rate of 20 mV S^{-1}. Current density was utilized to measure electrocatalytic activity, which was calculated from the ratio of the peak current and the surface area of Pt on Au-Ds.

2.5.3. Photoelectrochemistry

Photoelectrochemical properties were examined in a three-electrode quartz cell to facilitate the illumination of the photoelectrode surface. The illumination source was a 300-W Xe arc lamp (Newport, 66,901) directed at the quartz electrochemical cell (100 mW cm^{-2}) with an AM1.5G filter (Newport 81,094). A liquid filter (Newport, 6123NS) was used to avoid the heating of the solution by infrared light.

3. Results and discussion

XPS profiles revealed the electronic states of the chemical species on the Pt-modified Au-D/GCE surface. The XPS signals of Pt-modified Au-D/GCE were observed at binding energies of ~285, 86, and 75 eV after the reductive replacement of Cu, corresponding to the C 1*s*, Au 4*f*, and Pt 4*f* electron energy levels, respectively (Fig. 1(a)). High-resolution XPS measurements were conducted for examining the electronic states of Au and Pt on the GCE. As shown in the inset of Fig. 1(a), the Au 4*f* spectra were fitted with a pair of doublet peaks at 84.0 and 87.7 eV, corresponding to the $4f_{7/2}$and $4f_{5/2}$ levels of metallic Au, respectively. Binding energy signals were observed at 70.8 and 74.3 eV after the reductive replacement of Pt, corresponding to the Pt $4f_{7/2}$ and $4f_{5/2}$ electron energy levels, respectively. The binding energies for Au 4*f* and Pt 4*f* are consistent with the formation of the submonolayer Pt-modified Au surface [31]. Fig. 1(b) shows the XRD patterns of Pt-modified Au-Ds on GCE. All of the diffraction peaks well matched the Au FCC structure, indicative of high crystallinity [27]. Furthermore, other diffraction peaks were not observed, indicative of highly dispersed modified Pt atoms on Au-Ds. Fig. 1(c) shows the UV–Vis spectra of the prepared Au-Ds and Pt-modified Au-Ds. We observed a prominent absorption peak characteristic of the Au nanostructure at 495 nm, which corresponds to the SPR of Au-Ds. A ~10 nm red shift in the resonance as well as broadening of the peak was observed after Pt deposition [32]. This effect has been reported previously for unsupported Au nanoparticles covered with Pt. Fig. 1(d) and (e) show the SEM images of the prepared Pt-modified Au-D/GCE, which revealed a high density of structured Pt-modified Au-Ds deposited on GCE. The length of the Pt-modified Au-Ds

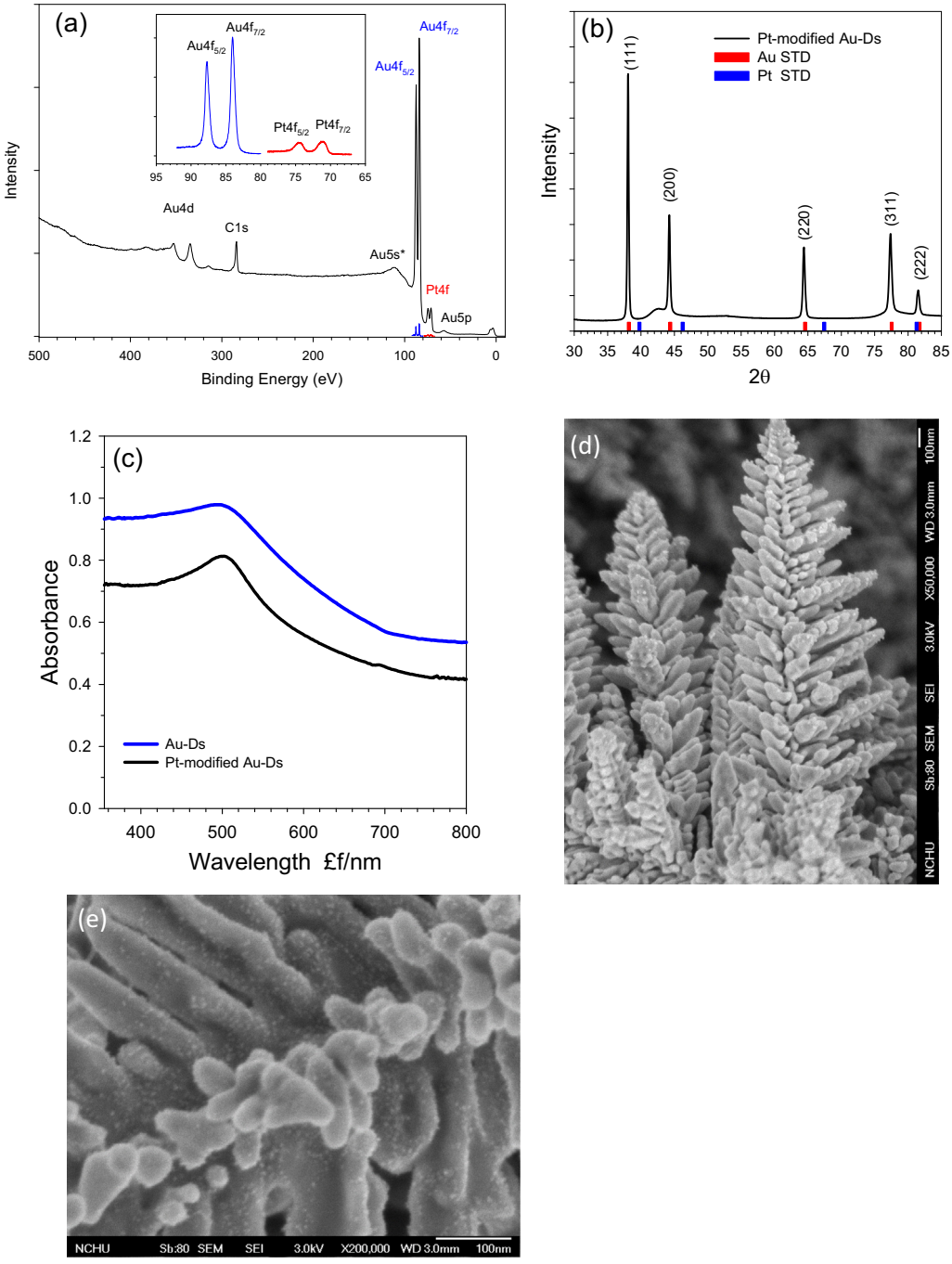

Fig. 1. (a) Typical XPS spectra of Au 4*f* and Pt 4*f* for Pt-modified Au-Ds. Inset: A photon energy of 580 eV was utilized to obtain XPS spectra. (b) Powder XRD patterns of Pt-modified Au-Ds. (c) Reflective UV–Vis absorption spectrum of Au-Ds and Pt-modified Au-Ds on a GCE. (d), and (e) SEM image of Pt-modified Au-Ds on a GCE.

was on the order of several micrometers, exhibiting a large, rough surface with several branches radially oriented away from the main stem. Numerous secondary leaves were observed on each branch, leading to Pt-modified Au dendrites.

The CV profiles of Au-Ds/GCE and Pt-modified Au-Ds/GCE in a N_2-saturated solution of 0.05 M H_2SO_4 solution at a scan rate of 50 mV/s were compared. Fig. 2 shows the Au-Ds oxidation/reduction peaks at ~1.23 V and 0.79 V, respectively. The deposition of Pt led to the decrease in the redox peaks of Au-Ds in the CV of Pt-modified Au-Ds, while typical redox peaks corresponding to Pt oxidation/reduction and hydrogen adsorption/desorption were gradually observed. The ECSAs of Au and Pt on Pt-modified Au plate or Au-Ds/GCE were estimated by coulombic integration of the cathodic peak current at 0.79 V and the hydrogen adsorption/desorption in the lower potential region, respectively. Hence, the ECSA of Au-Ds is ~58.7 cm^2, based on a scaling constant S of 400 μC cm^{-2} [26]. The Au-D surface was gradually covered by the deposited Pt atoms. The ECSA of Au-Ds decreased from 58.7 to 44.8 cm^2, while that of Pt reached 34.2 cm^2. In addition, the ECSA of Pt on the Pt-modified Au plate was 16.95 cm^2. Hence, the combined results from UV–Vis spectroscopy, SEM, XRD, XPS, and CV measurements indicated that numerous Pt-modified crystalline hyperbranched Au-Ds are observed on the GCE.

Fig. 3(a) shows the electrocatalytic activities for the FAOR of Pt wire, Au-Ds, Pt-modified Au plate and Pt-modified Au-Ds in a mixed solution of 0.50 M formic acid + 0.5 M H_2SO_4 in the dark. Au-Ds/GCE exhibited a nearly negligible activity toward the FAOR as has been

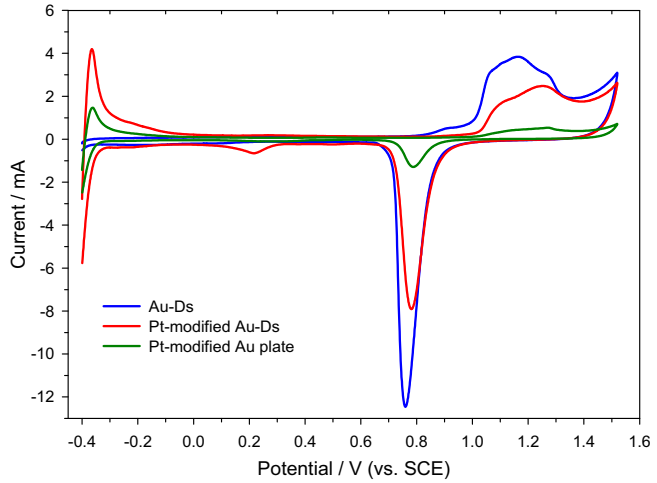

Fig. 2. CV profiles recorded at 50 mV/s for Au-D/GCE, Pt-modified Au plate, and Pt-modified Au-D/GCE in a N_2-saturated solution of 0.5 M H_2SO_4(aq). Scan rate: 50 mV/s. The GCE area is ~0.4 cm^2.

reported previously [16,17]. For Pt-modified Au plate and Pt-modified Au-Ds, the only oxidation current density peak at 0.27 V corresponded to the direct oxidation of formic acid to carbon dioxide, implying that the FAOR mainly occurs via the dehydrogenation pathway. In contrast to the dehydration pathway, the oxidation current was possibly observed at 0.65 V on Pt-wire (Fig. 3(a) dark red curve). The current densities were normalized to the ECSA values for Pt measured by integrating the charge involved in hydrogen adsorption/desorption, as described above (Fig. 3(b)). For Pt-modified Au plate and Pt-modified Au-Ds/GCE, the forward current density were almost equivalent to the reverse current, indicative of an equivalent oxidation activity during forward and backward sweep [33]. From the maximum forward and reverse currents obtained, the adsorbed CO poisoning species does not play a major role in decreasing current of Pt-modified Au-Ds during the forward scan. Notably, Au-D nanostructures exhibit an enhanced surface-area-to-volume ratio and provide considerable access to electrochemical reactants. The catalytic activity of the Pt-modified Au-Ds is twice that of Pt-modified Au plate.

In this study using the Pt-modified Au-D catalyst, the current densities were sensitive to the formic acid concentration in a 0.5 M H_2SO_4 solution at 25 °C (Fig. 4(a)). All of the CV profiles were obtained at similar low onset potentials, i.e., −0.1 V. The maximum current densities increased with the formic acid concentrations between 0.1 and 0.5 M at 0.23 V. Fig. 4(b) shows the Tafel plots of Pt-modified Au-D catalysts: All plots exhibited a good linear relationship in the low current region. Tafel plots revealed a linear region between −80 and 30 mV with a slope of ~90 mV dec^{-1}. A low Tafel slope value of ~90 mV dec^{-1} was found to be an indicator of a dominant dehydrogenation pathway, which was consistent with the result obtained from CV curves [2,15]. Moreover, CV curves were recorded for the FAOR on Pt-modified Au-Ds in a 0.5 M H_2SO_4 solution containing various formic acid concentrations in the Tafel region. Results revealed a linear dependence between log i and log [FA], with a slope of 1 ± 0.05, indicating that the reaction is first order with respect to formic acid in the 0.5 M H_2SO_4 solution.

Fig. 5(a) shows the temperature dependence of the FAOR over Pt-modified Au-Ds at 25–45 °C at a scan rate 20 mV/s. With increasing temperature, the oxidation current density increased, revealing enhanced activities. With the increase in the temperature from 25 to 45 °C, current densities increased by 2.3 times at 0.23 V for the FAOR over Pt-modified Au-Ds. Fig. 5(b) shows the measured k_{obs} values on this electrode at three representative temperatures in the Tafel region. Linear relationships were observed between ln k_{obs} and inverse temperature, indicating that the reaction pathway at each potential does not change with temperature. The apparent activation energy for the FAOR over Pt-modified Au-Ds in this region was ~35.4 kJ mol^{-1}. A majority of the previously reported activation energies for the FAOR range from 40 to 100 kJ mol^{-1} [8,25]. The apparent lower activation energy of ≤40 kJ mol^{-1} is possibly related to oxidation mainly occurring via the dehydrogenation pathway.

Furthermore, the SPR effect of Pt-modified Au-Ds for the FAOR was investigated. The effect of the formic acid concentration was examined in a 0.5 M H_2SO_4 solution by using 0.05–0.5 M formic acid under AM 1.5G illumination at 100 mW cm^{-2} (Fig. 6(a)). CV profiles revealed that with increasing formic acid concentration, the maximum current densities apparently increased from 0.10 to 1.66 mA cm^{-2} at 0.23 V. On the other hand, the Tafel plots shown in Fig. 6(b) exhibited a linear region between −80 and 20 mV with a slope of ~90 mV dec^{-1}, indicating that the FAOR still obeys the dehydrogenation pathway under AM 1.5G illumination. Fig. 6(c) shows the current densities as a function of the formic acid concentration at a constant potential in the Tafel region. Current densities increased with the formic acid concentration up to 0.3 M. Fitting a line with a slope equal to 1 implied a first-order reaction with respect to formic acid in the electrolytes containing < 0.3 M formic acid. In addition, a similar concentration dependence was observed without AM 1.5G illumination (Fig. 4(c)). The rate for the FAOR increased to 68% at 25 °C under AM 1.5G illumination compared to dark conditions. A further increase in the formic acid concentration led

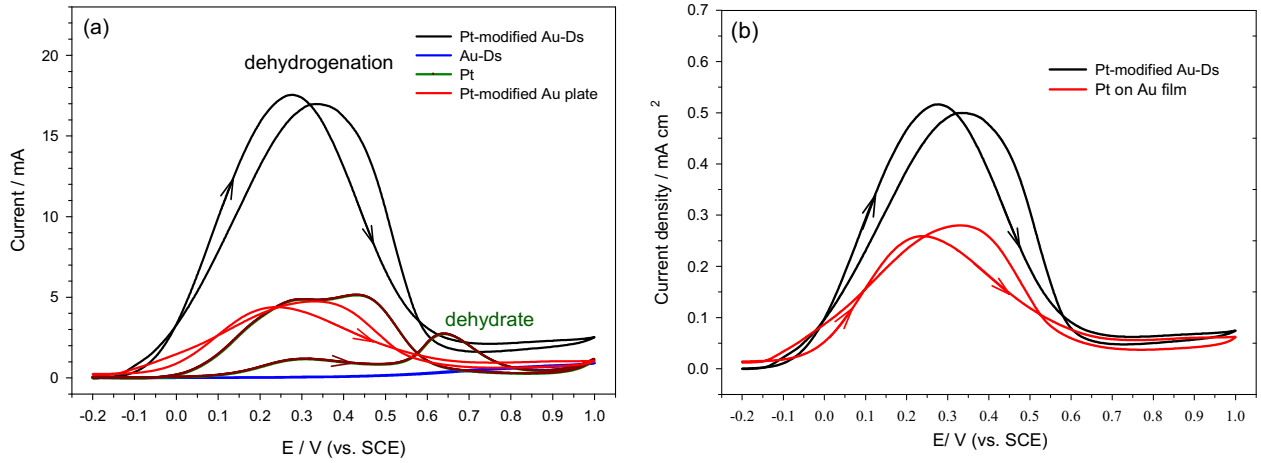

Fig. 3. (a) CV profiles of Pt wire, Au-Ds Pt-modified Au plate and Pt-modified Au-D/GCE saturated with N_2 in a solution of 0.50 M formic acid + 0.5 M H_2SO_4 at 25 °C in the dark. Scan rate: 20 mVs^{-1}. (b) Normalized CV profiles of Pt-modified Au plate and Au-D/GC saturated with N_2 in a solution of 0.50 M formic acid + 0.5 M H_2SO_4 at 25 °C.

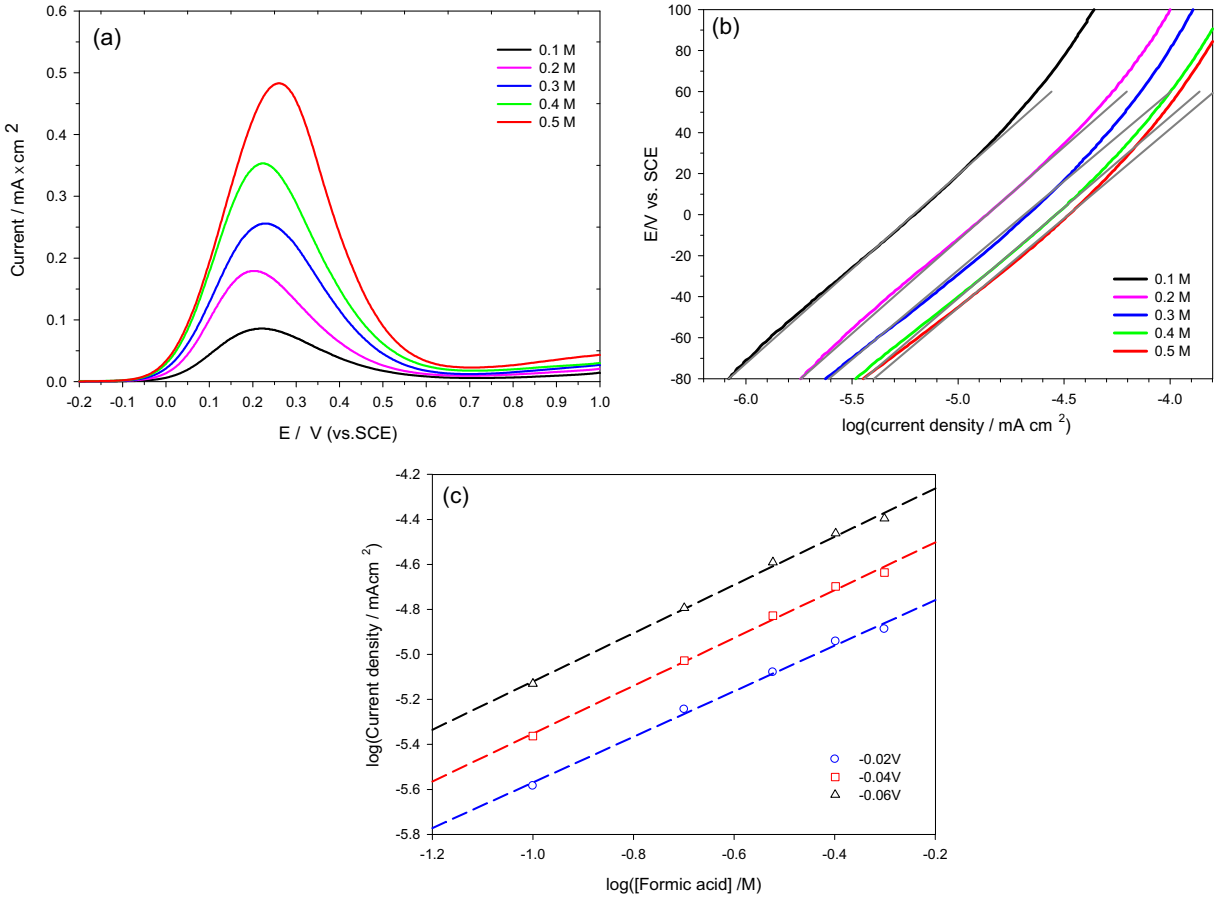

Fig. 4. (a) Concentration-dependent CV profiles of formic acid electrooxidation on Pt-modified Au-D/GCE in a 0.5 M H_2SO_4 solution at 25 °C. Scan rate: 20 mV/s. (b) Tafel plots for formic acid oxidation reaction. (c) Dependence of current density on the formic acid concentration in a 0.5 M H_2SO_4 solution at 25 °C. Data taken from the Tafel lines at the potential indicated on the diagram.

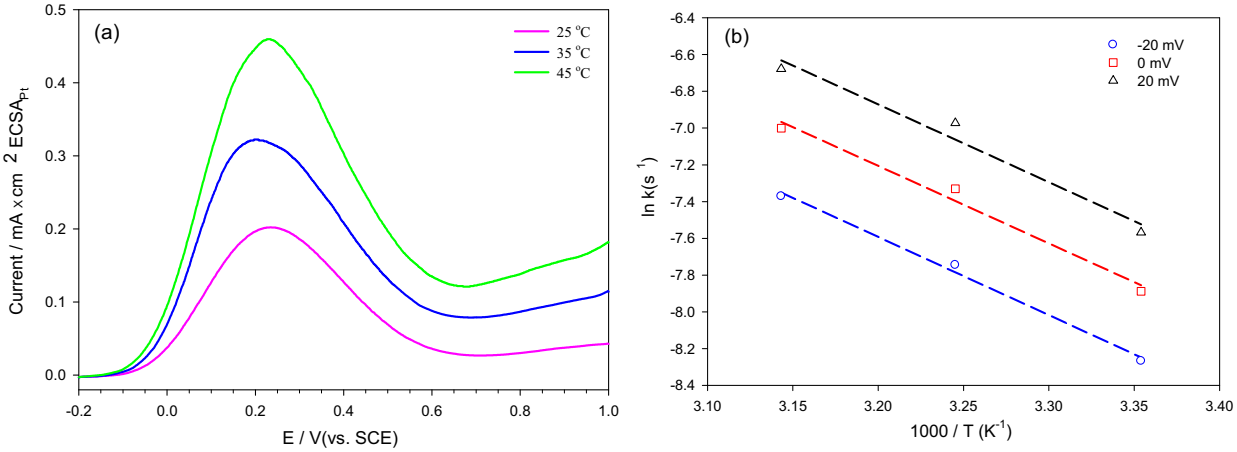

Fig. 5. (a) CV profiles for 0.2 M formic acid in 0.5 M H_2SO_4 on Pt-modified Au-D/GCE at 25, 35, and 45 °C. (b) Arrhenius plots at different potentials for the formic acid oxidation on Pt-modified Au-D/GCE. Data taken from the Tafel region at the potential indicated on the diagram.

to an almost constant current density in the Tafel region. In the solution containing > 0.3 M formic acid, the expected Pt-modified Au-D surface available for the intermediate reached saturation, and the further increase in the formic acid concentration did not lead to the increase of the current density under AM 1.5G illumination at 100 mW cm^{-2}.

Hence, the enhanced catalytic activity is confirmed to be induced by the SPR effect, and catalysis follows the same dehydrogenation pathway under dark conditions. Next, the dependence of the catalytic activity on photon irradiation was systematically investigated by the chronoamperograms recorded using an AM 1.5G filter with a power density of 100 mW cm^{-2} in a 0.5 M formic acid + 0.5 M H_2SO_4 solution at 0.26 V for 2000 s (Fig. 7(a)). The polarization current for FAOR under all chronoamperograms recorded conditions remarkably decays initially and reaches a stable value after polarization at 0.26 V. Subsequently, gradual and continuous current decay is commonly observed in the chronoamperograms of oxidation of formic acid in several media with Pt as the anode. This effect is most likely due to the presence of other contaminating agents such as sulfates and other anions [34]. The

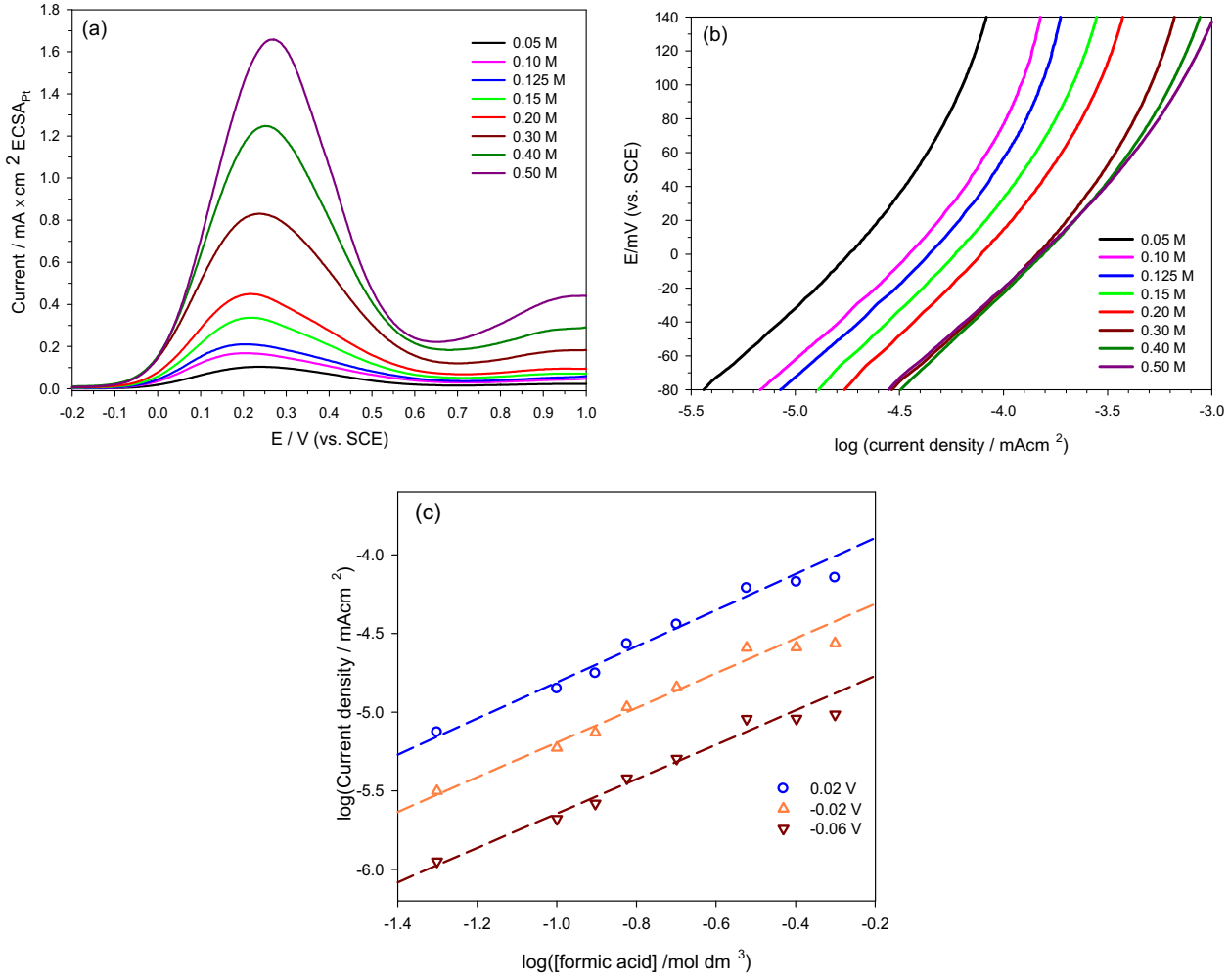

Fig. 6. (a) Concentration-dependent CV profiles of formic acid photo electrooxidation on Pt-modified Au-D/GCE in a 0.5 M H_2SO_4 solution under AM1.5G illumination at 25 °C. Scan rate was 20 mV/s. (b) Tafel plots for the formic acid oxidation reaction and (c) Dependence of current density on the formic acid concentration in a 0.5 M H_2SO_4 solution under AM1.5G illumination at 25 °C. Data were taken from the Tafel lines at the potential indicated on the diagram.

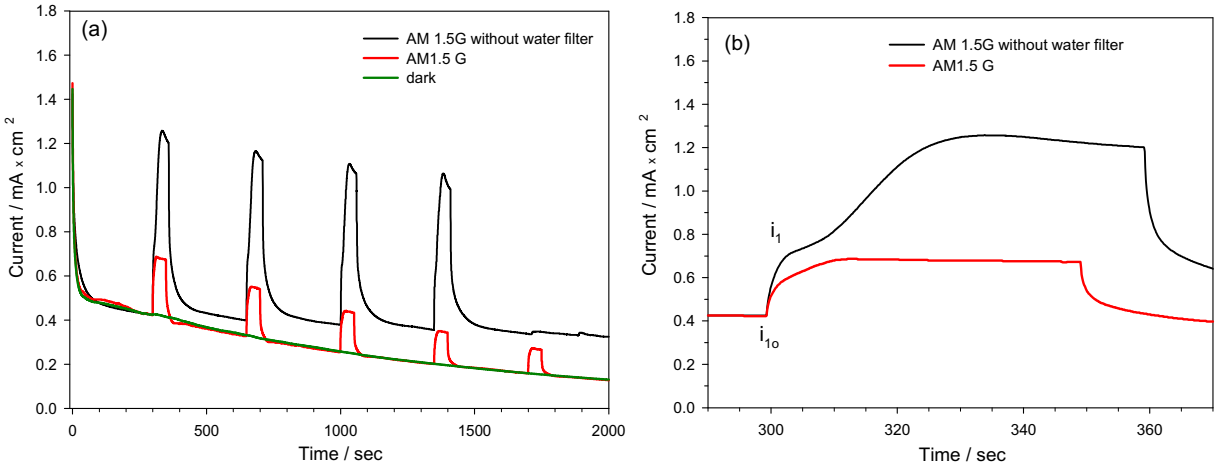

Fig. 7. (a) Chronoamperograms during the light on/off test for Pt-modified Au-Ds under AM1.5G light (with/without a water filter) illumination and dark in a 0.50 M formic acid + 0.50 M H_2SO_4 solution at 0.26 V, which was maintained for 2000 s. Illumination power densities on the working electrode were 100 and 140 mW/cm^2, respectively. (b) the first cycle chronoamperograms during light on/off test.

current density immediately increased during the first several seconds (≤5 s) after illumination for the chronoamperogram recorded at 25 °C. The contribution ratio for the photo-enhanced electrocatalytic effect would be $[(i_n - i_{no})/i_n]$, where n = 1, 2, 3…etc. (Fig. 7(b)) [35]. The contribution ratio for the average photo electrocatalytic effect was calculated to be ~40% for the Pt-modified Au-Ds at 25 °C. Owing to the SPR effect, Au-Ds exhibited strong absorption in the visible-light region (Fig. 1(c)). After photoirradiation, the immediate current increase was

caused by the photo-enhanced electrocatalytic effect [36]. Simultaneously, the photo-thermal effect of nanostructured metals is related to the conversion of absorbed photon energy into heat [37]. Therefore, the current density for the formic acid oxidation reaction further increases during irradiation before 10 s. When the exposure time exceeded 10 s, the reaction was maintained in the steady state. When AM 1.5G light was turned off, the current density for the FAOR decreased to the trend of unirradiation. On removing the water filter, highly photoenhanced FAOR was observed under irradiation at AM 1.5G with a power density of 140 mW cm^{-2} in a 0.5 M formic acid + 0.5 M H_2SO_4 solution at 0.26 V for 2000 s. The calculated contribution ratio of the photoelectrocatalytic effect was approximately 48% [(8.16–4.21)/8.16] for the Pt-modified Au-D. After illumination for 10 s, the current density began to increase with the gradual increase in temperature due to the photothermal effect of the irradiation [35]. The photo and photo-thermal effect further considerably boosted the catalyst activity to ~67% [(12.58–4.21)/12.58] under irradiation with AM 1.5G without a water filter.

4. Conclusions

A Pt-modified Au-D catalyst with excellent performance for the formic acid oxidation reaction (FAOR) was prepared by a simple electrochemical method. The catalyst was characterized by UV/Vis spectroscopy, XPS, XRD, SEM, and CV measurements, and the fabricated submonolayer Pt-modified Au-D catalyst exhibited an extensive surface area and minimized the amount of Pt on the crystalline hyperbranched Au-D surface. Pt-modified Au-Ds facilitated the FAOR via the dehydrogenation pathway and clearly suppressed the dehydration pathway with a low activation energy of 35.4 kJ mol^{-1}. Moreover, the oxidation reaction on Pt-modified Au-Ds was first order with respect to formic acid. The catalytic activity of Pt-modified Au-Ds toward the FAOR was considerably enhanced by the SPR generated photoelectrocatalytic and photo-thermal effect under AM 1.5G illumination. Notably, the FAOR followed the same pathway, i.e., dehydrogenation pathway, under illumination. The photoelectrocatalytic effect on the Pt-modified Au-Ds quantitatively increased by 68% in the Tafel region. Finally, the chronoamperometric current was utilized to evaluate the stability and photoelectrocatalytic activity of Pt-modified Au-Ds. These results clearly demonstrated a simple method for synthesizing a stable, durable catalyst with a low activation energy for the FAOR. Overall results revealed that the unique role of photo-active Pt-modified Au-Ds needs to be further investigated. These findings suggested that our approach can be extended to investigate other photoelectric catalysts for further understanding and improving the DFAFC system.

Acknowledgments

This work has been financially supported by the Ministry of Science and Technology, Taiwan (MOST 106-2113-M-029-007 and MOST 106-2632-M-029-001) and Tunghai University.

References

[1] J. Joo, T. Uchida, A. Cuesta, M.T.M. Koper, M. Osawa, Importance of acid–base equilibrium in electrocatalytic oxidation of formic acid on platinum, J. Am. Chem. Soc. 135 (2013) 9991–9994.
[2] M.D. Obradović, A.V. Tripković, S.L. Gojković, The origin of high activity of Pt–Au surfaces in the formic acid oxidation, Electrochim. Acta 55 (2009) 204–209.
[3] X. Jiang, X. Yan, W. Ren, Y. Jia, J. Chen, D. Sun, L. Xu, Y. Tang, Porous AgPt@Pt nanooctahedra as an efficient catalyst toward formic acid oxidation with predominant dehydrogenation pathway, ACS Appl. Mater. Interfaces 8 (2016) 31076–31082.
[4] X. Yu, P.G. Pickup, Recent advances in direct formic acid fuel cells (DFAFC), J. Power Sources 182 (2008) 124–132.
[5] I.-S. Park, K.-S. Lee, J.-H. Choi, H.-Y. Park, Y.-E. Sung, Surface structure of Pt-modified au nanoparticles and electrocatalytic activity in formic acid electro-oxidation, J. Phys. Chem. C 111 (2007) 19126–19133.
[6] A. Ferre-Vilaplana, J.V. Perales-Rondón, C. Buso-Rogero, J.M. Feliu, E. Herrero, Formic acid oxidation on platinum electrodes: a detailed mechanism supported by experiments and calculations on well-defined surfaces, J. Mater. Chem. A 5 (2017) 21773–21784.
[7] Y. Kang, L. Qi, M. Li, R.E. Diaz, D. Su, R.R. Adzic, E. Stach, J. Li, C.B. Murray, Highly active Pt3Pb and core–shell Pt3Pb–Pt electrocatalysts for formic acid oxidation, ACS Nano 6 (2012) 2818–2825.
[8] G. Xiaohu, C. Xiao, D. Yi, Platinum-decorated Au porous nanotubes as highly efficient catalysts for formic acid electro-oxidation, ChemPhysChem 11 (2010) 841–846.
[9] S.-W. Ting, S. Cheng, K.-Y. Tsang, N. van der Laak, K.-Y. Chan, Low activation energy dehydrogenation of aqueous formic acid on platinum–ruthenium–bismuth oxide at near ambient temperature and pressure, Chem. Commun. (2009) 7333–7335.
[10] R. Zeng, Z. Luo, L. Zhang, D. Tang, Platinum nanozyme-catalyzed gas generation for pressure-based bioassay using polyaniline nanowires-functionalized graphene oxide framework, Anal. Chem. 90 (2018) 12299–12306.
[11] J. Zhou, J. Zhuang, M. Miró, Z. Gao, G. Chen, D. Tang, Carbon nanospheres-promoted electrochemical immunoassay coupled with hollow platinum nanolabels for sensitivity enhancement, Biosens. Bioelectron. 35 (2012) 394–400.
[12] Z. Gao, H. Ye, D. Tang, J. Tao, S. Habibi, A. Minerick, D. Tang, X. Xia, Platinum-decorated gold nanoparticles with dual functionalities for ultrasensitive colorimetric in vitro diagnostics, Nano Lett. 17 (2017) 5572–5579.
[13] Z. Gao, S. Lv, M. Xu, D. Tang, High-index {hk0} faceted platinum concave nanocubes with enhanced peroxidase-like activity for an ultrasensitive colorimetric immunoassay of the human prostate-specific antigen, Analyst 142 (2017) 911–917.
[14] Y. Xia, J. Liu, W. Huang, Z. Li, Electrochemical fabrication of clean dendritic Au supported Pt clusters for electrocatalytic oxidation of formic acid, Electrochim. Acta 70 (2012) 304–312.
[15] Q. Zhang, R. Yue, F. Jiang, H. Wang, C. Zhai, P. Yang, Y. Du, Au as an efficient promoter for electrocatalytic oxidation of formic acid and carbon monoxide: a comparison between Pt-on-Au and PtAu alloy catalysts, Gold Bull. 46 (2013) 175–184.
[16] Z. Huang, Y. Liu, F. Xie, Y. Fu, Y. He, M. Ma, Q. Xie, S. Yao, Au-supported Pt–Au mixed atomic monolayer electrocatalyst with ultrahigh specific activity for oxidation of formic acid in acidic solution, Chem. Commun. 48 (2012) 12106–12108.
[17] N. Kristian, Y. Yan, X. Wang, Highly efficient submonolayer Pt-decorated Au nanocatalysts for formic acid oxidation, Chem. Commun. (2008) 353–355.
[18] S.H. Ahn, Y. Liu, T.P. Moffat, Ultrathin platinum films for methanol and formic acid oxidation: activity as a function of film thickness and coverage, ACS Catal. 5 (2015) 2124–2136.
[19] Z. Zheng, T. Tachikawa, T. Majima, Plasmon-enhanced formic acid dehydrogenation using anisotropic Pd–Au nanorods studied at the single-particle level, J. Am. Chem. Soc. 137 (2015) 948–957.
[20] F.-H. Cho, S.-C. Kuo, Y.-H. Lai, Surface-plasmon-induced azo coupling reaction between nitro compounds on dendritic silver monitored by surface-enhanced Raman spectroscopy, RSC Adv. 7 (2017) 10259–10265.
[21] Z. Zheng, T. Tachikawa, T. Majima, Single-particle study of Pt-modified Au nanorods for plasmon-enhanced hydrogen generation in visible to near-infrared region, J. Am. Chem. Soc. 136 (2014) 6870–6873.
[22] G.-R. Zhang, D. Zhao, Y.-Y. Feng, B. Zhang, D.S. Su, G. Liu, B.-Q. Xu, Catalytic Pt-on-Au nanostructures: why Pt becomes more active on smaller Au particles, ACS Nano 6 (2012) 2226–2236.
[23] S.R. Brankovic, J.X. Wang, R.R. Adžić, Metal monolayer deposition by replacement of metal adlayers on electrode surfaces, Surf. Sci. 474 (2001) L173–L179.
[24] Z. Al Amri, M.P. Mercer, N. Vasiljevic, Surface limited redox replacement deposition of platinum ultrathin films on gold: thickness and structure dependent activity towards the carbon monoxide and formic acid oxidation reactions, Electrochim. Acta 210 (2016) 520–529.
[25] P.A. Ganesh, D. Jeyakumar, Intriguing catalytic activity of surface active gold-platinum islands on nano-porous au in determining efficient direct formic acid oxidation pathway, ChemistrySelect 2 (2017) 3562–3571.
[26] Y.-H. Lai, S.-C. Kuo, Y.-C. Hsieh, Y.-C. Tai, W.-H. Hung, U.S. Jeng, Electrochemically fabricated gold dendrites with underpotential deposited silver monolayers for a bimetallic SERS-active substrate, RSC Adv. 6 (2016) 13185–13192.
[27] F.-H. Cho, Y.-C. Lin, Y.-H. Lai, Electrochemically fabricated gold dendrites with high-index facets for use as surface-enhanced Raman-scattering-active substrates, Appl. Surf. Sci. 402 (2017) 147–153.
[28] T.-H. Lin, C.-W. Lin, H.-H. Liu, J.-T. Sheu, W.-H. Hung, Potential-controlled electrodeposition of gold dendrites in the presence of cysteine, Chem. Commun. 47 (2011) 2044–2046.
[29] C.-Y. Chang, Y.-C. Hsieh, Y.-Y. Huang, Y.-J. Wang, Y.-M. Chen, Y.-B. Huang, W.-H. Hung, Y.-H. Lai, Effect of chemical surface modification on dendritic gold in surface-enhanced Raman scattering-active substrates, J. Raman Spectrosc. 0 (2019) 1–8.
[30] Y.-F. Song, C.-H. Chang, C.-Y. Liu, S.-H. Chang, U.S. Jeng, Y.-H. Lai, D.-G. Liu, S.-C. Chung, K.-L. Tsang, G.-C. Yin, J.-F. Lee, H.-S. Sheu, M.-T. Tang, C.-S. Hwang, Y.-K. Hwu, K.S. Liang, X-ray beamlines for structural studies at the NSRRC superconducting wavelength shifter, J. Synchrotron Radiat. 14 (2007) 320–325.
[31] D. Zhao, B.-Q. Xu, Platinum covering of gold nanoparticles for utilization enhancement of Pt in electrocatalysts, Phys. Chem. Chem. Phys. 8 (2006) 5106–5114.
[32] J.U. Salmón-Gamboa, M. Romero-Gómez, D.J. Roth, M.J. Barber, P. Wang, S.M. Fairclough, M.E. Nasir, A.V. Krasavin, W. Dickson, A.V. Zayats, Optimizing hot carrier effects in Pt-decorated plasmonic heterostructures, Faraday Discuss. (2019), https://doi.org/10.1039/C8FD00150B.
[33] Y. Wang, Q. He, H. Wei, J. Guo, K. Ding, Q. Wang, Z. Wang, S. Wei, Z. Guo, Optimal electrocatalytic Pd/MWNTs nanocatalysts toward formic acid oxidation,

Electrochim. Acta 184 (2015) 452–465.
[34] J.V. Perales-Rondón, E. Herrero, J.M. Feliu, Effects of the anion adsorption and pH on the formic acid oxidation reaction on Pt(111) electrodes, Electrochim. Acta 140 (2014) 511–517.
[35] Y. Hao, H. Lan-Qi, H. Yu-Wen, L. Xihong, L. Gao-Ren, L. Biju, R. Bin, T. Yexiang, F. Ping-Ping, Quantitative detection of photothermal and photoelectrocatalytic effects induced by SPR from Au@Pt nanoparticles, Angew. Chem. Int. Ed. 54 (2015) 11462–11466.
[36] S. Chavez, U. Aslam, S. Linic, Design principles for directing energy and energetic charge flow in multicomponent plasmonic nanostructures, ACS Energy Letters 3 (2018) 1590–1596.
[37] H. Yang, L.-Q. He, Z.-H. Wang, Y.-Y. Zheng, X. Lu, G.-R. Li, P.-P. Fang, J. Chen, Y. Tong, Surface plasmon resonance promoted photoelectrocatalyst by visible light from Au core Pd shell Pt cluster nanoparticles, Electrochim. Acta 209 (2016) 591–598.